Bending and free vibration analysis of a smart functionally graded plate

Z. G. Bian[†]

Department of Civil Engineering, Zhejiang University, Hangzhou 310027, P. R. China
(State Key Lab of CAD & CG, Zhejiang University, Hangzhou 310027, P. R. China
Department of Construction Engineering, Ningbo Institute of Technology, Zhejiang University,
Ningbo 315100, P. R. China)

J. Ying[‡]

Department of Mechanical Engineering, Zhejiang University, Hangzhou 310027, P. R. China

W. Q. Chen[‡†]

Department of Civil Engineering, Zhejiang University, Hangzhou 310027, P. R. China
(State Key Lab of CAD & CG, Zhejiang University, Hangzhou 310027, P. R. China)

H. J. Ding[‡‡]

Department of Civil Engineering, Zhejiang University, Hangzhou 310027, P. R. China

Abstract. A simply supported hybrid plate consisting of top and bottom functionally graded elastic layers and an intermediate actuating or sensing homogeneous piezoelectric layer is investigated by an elasticity (piezoelasticity) method, which is based on state space formulations. The general spring layer model is adopted to consider the effect of bonding adhesives between the piezoelectric layer and the two functionally graded ones. The two functionally graded layers are inhomogeneous along the thickness direction, which are approached by laminate models. The effect of interlaminar bonding imperfections on the static bending and free vibration of the smart plate is discussed in the numerical examples.

Keywords: functionally graded material; piezoelectric layer; state space approach; spring layer model.

1. Introduction

Research on embedded piezoelectric sensors/actuators has shown great advantages over the

---
† Dr., E-mail: bianzuguang@hotmail.com
‡ Associate Professor, E-mail: yingji@zju.edu.cn
‡† Professor, Corresponding author, E-mail: chenwq@ccea.zju.edu.cn
‡‡ Professor, E-mail: dinghj@zju.edu.cn

traditional surface-bounded ones. The most prominent feature is that damages of surface bonded sensors/actuators due to contact with surrounding objects can be avoided in the embedded case (Vel and Batra 2001, Ali *et al.* 2004, Batra and Liang 1997). Saravanos and Heyliger (1995) employed a layerwise linear theory to analyze composite beams with embedded piezoelectric sensors. Based on a high order displacement field and a layerwise linear electric potential, Chee *et al.* (2001, 2002) developed a finite element method and investigated the static shape control of adaptive composite plates. Roh and Kim (2003) incorporated the finite element method with the first-order shear deformation theory of plates to study the dynamic response and adaptability of hybrid smart composite plates under low velocity impact.

In the works mentioned above, the interfacial bonding was assumed to be perfect, which is not always the case in practice. During the process of fabrication or the service life, some interfacial imperfections may be induced. To prevent laminates from shear failure, weak bonding is artificially introduced, hereby reducing the concentration of transverse shear stresses. Thus, studies on laminates with imperfect interfaces have gained more and more attentions. Cheng and Batra (2001) investigated thermal effects on imperfectly bonded laminated composite shells. Rokhlin *et al.* (2004) developed an ultrasonic experimental method to evaluate imperfect interfaces and adhesive bonds. To model the interfacial imperfection, a linear interface model suggested by Aboudi (1987) has been widely employed since it can simply and effectively describe the important features of weak interfaces (Meguid and Wang 1999, Cheng and Kitipornchai 2000, Icardi *et al.* 2000, Chen and Lee 2004a, Chen *et al.* 2004a, Cai *et al.* 2004).

In the present paper, a general linear spring-layer model (Chen *et al.* 2003a, Chen and Lee 2004b, Chen *et al.* 2004b,c,d) is employed to characterize the imperfect behavior of interfaces in a smart structure consisting of two functional graded elastic layers weekly bond with the top and bottom surfaces of a piezoelectric plate, which acts as either sensor or actuator. Functional graded materials (FGMs) are a kind of inhomogeneous materials whose volume fractions of the constituents and thus the mechanical properties vary continuously over a macroscale geometrical dimension. Differing from the conventional laminated materials, FGMs do not possess discernible internal phase boundaries, which directly results to slight stress concentration caused by kinds of external loads (Li and Weng 2002). So FGMs are widely applied in various engineering including electron, chemistry, optics, biomedicine, etc. (Koizumi 1997). As an important member of adaptive structures, FGMs bonded with piezoelectric actuators or sensors have abstracted much attention recently (He *et al.* 2001, Liew *et al.* 2001, 2003, Yang *et al.* 2004, Shen and Liew 2004). Among these literatures, some conventional simplified assumptions on the mechanical displacements and electric potential were introduced, which should be carefully clarified by three dimensional analyses. Ootao and Tanigawa (2000) studied an FGM rectangular plate bonded to a piezoelectric plate in a thermal environment. They employed a three dimensional method similar to Pagano (1969) incorporated with a laminated model to approximate the FGM plate. Such a method, however, will become time-consuming when the divided number of laminated model increases for results of high accuracy (Cai *et al.* 2004, Chen and Lee 2004b, Noor and Burton 1990).

In this paper, another three-dimensional method, i.e., the state space method (SSM), is employed. Since the scale of final solving equations is independent of layers involved in laminates, the SSM possesses superiority in analyzing laminated structures (Bahar 1975, Lee and Jiang 1996, Chen *et al.* 2003b, 2004e, Deu and Benjeddou 2005). Recently, Chen and Lee (2004a,b), Chen *et al.* (2003a, 2004a,b,c,d) applied the SSM to obtain benchmark solutions of laminated beams, plates and cylindrical panels with imperfect interfaces. These solutions construct a solid base for clarifying
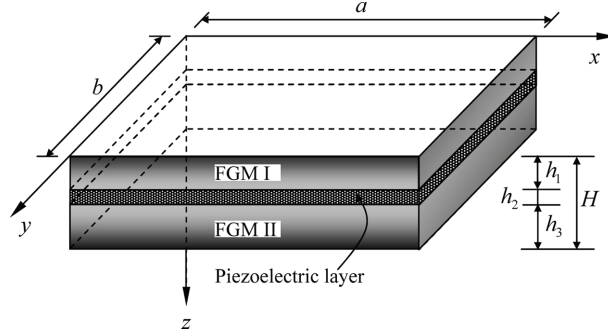
Fig. 1 Geometry and coordinates of a smart plate

one-dimensional beam theories and two-dimensional plate/shell theories as well as numerical methods such as FEM and BEM. As an extension of these works, the present paper deals with the static bending and free vibration of a smart hybrid FGM plate. The effects of some parameters including the gradient index of FGMs and compliance coefficients of weak interfaces are discussed in the numerical examples. It is noted that a thorough understanding of the effect of bonding imperfection can not only help us to predict correctly the health condition of a host structure from the measured signals, but also extend the service lifetime of the actuators/sensors if the bonding property is well characterized.

2. State space method

We consider a smart plate in Fig. 1. The two FGM elastic layers, FGM I and FGM II, are connected with an intermediate actuating or sensing piezoelectric layer, which is homogeneous.

2.1 Formulations for piezoelectric layer

The basic equations of orthotropic piezoelectric materials polarized in the z direction (Ding and Chen 2001) are

Generalized constitutive relations:

$$\sigma_{xx} = c_{11}\frac{\partial u_x}{\partial x} + c_{12}\frac{\partial u_y}{\partial y} + c_{13}\frac{\partial u_z}{\partial z} + e_{31}\frac{\partial \phi}{\partial z}, \quad \sigma_{yy} = c_{12}\frac{\partial u_x}{\partial x} + c_{22}\frac{\partial u_y}{\partial y} + c_{23}\frac{\partial u_z}{\partial z} + e_{32}\frac{\partial \phi}{\partial z}$$

$$\sigma_{xy} = c_{66}\left(\frac{\partial u_x}{\partial y} + \frac{\partial u_y}{\partial x}\right), \quad \sigma_{zz} = c_{13}\frac{\partial u_x}{\partial x} + c_{23}\frac{\partial u_y}{\partial y} + c_{33}\frac{\partial u_z}{\partial z} + e_{33}\frac{\partial \phi}{\partial z}$$

$$\sigma_{zx} = c_{55}\left(\frac{\partial u_x}{\partial z} + \frac{\partial u_z}{\partial x}\right) + e_{15}\frac{\partial \phi}{\partial x}, \quad \sigma_{yz} = c_{44}\left(\frac{\partial u_y}{\partial z} + \frac{\partial u_z}{\partial y}\right) + e_{24}\frac{\partial \phi}{\partial y} \quad (1)$$

$$D_x = e_{15}\left(\frac{\partial u_x}{\partial z} + \frac{\partial u_z}{\partial x}\right) - \varepsilon_{11}\frac{\partial \phi}{\partial x}, \quad D_y = e_{24}\left(\frac{\partial u_y}{\partial z} + \frac{\partial u_z}{\partial y}\right) - \varepsilon_{22}\frac{\partial \phi}{\partial y}$$

$$D_z = e_{31}\frac{\partial u_x}{\partial x} + e_{32}\frac{\partial u_y}{\partial y} + e_{33}\frac{\partial u_z}{\partial z} - \varepsilon_{33}\frac{\partial \phi}{\partial z}$$

Governing equations:

$$\frac{\partial \sigma_{xx}}{\partial x} + \frac{\partial \sigma_{xy}}{\partial y} + \frac{\partial \sigma_{zx}}{\partial z} = \rho \frac{\partial^2 u_x}{\partial t^2}, \quad \frac{\partial \sigma_{xy}}{\partial x} + \frac{\partial \sigma_{yy}}{\partial y} + \frac{\partial \sigma_{yz}}{\partial z} = \rho \frac{\partial^2 u_y}{\partial t^2}$$

$$\frac{\partial \sigma_{zx}}{\partial x} + \frac{\partial \sigma_{yz}}{\partial y} + \frac{\partial \sigma_{zz}}{\partial z} = \rho \frac{\partial^2 u_z}{\partial t^2}, \quad \frac{\partial D_x}{\partial x} + \frac{\partial D_y}{\partial y} + \frac{\partial D_z}{\partial z} = 0$$

(2)

The state equations can be directly derived from Eqs. (1) and (2) by choosing the state vector as $\mathbf{V} = [u_x \; u_y \; \sigma_{zz} \; D_z \; \sigma_{zx} \; \sigma_{yz} \; u_z \; \phi]^T$

$$\partial \mathbf{V} / \partial z = \mathbf{M} \mathbf{V} \tag{3}$$

where the operator matrix $\mathbf{M}$ is given in Appendix A. In addition, we have

$$\Theta = \mathbf{N} \mathbf{V} \tag{4}$$

where $\Theta = [\sigma_{xx} \; \sigma_{yy} \; \sigma_{xy} \; D_x \; D_y]^T$ is the deduced vector, and $\mathbf{N}$ is also an operator matrix presented in Appendix A.

The simply supported conditions for a piezoelectric plate (Ding and Chen 2001) are

$$\sigma_{xx} = u_z = u_y = \phi = 0, \text{ at } x = 0 \text{ or } a, \quad \sigma_{yy} = u_z = u_y = \phi = 0, \text{ at } y = 0 \text{ or } b \tag{5}$$

To satisfy these boundary conditions, the following Fourier expansions are applied

$$\begin{Bmatrix} u_x \\ u_y \\ \sigma_{zz} \\ D_z \\ \sigma_{zx} \\ \sigma_{yz} \\ u_z \\ \phi \end{Bmatrix} = \sum_{m=1}^{\infty} \sum_{n=1}^{\infty} \begin{Bmatrix} H \bar{u}_x(\zeta) \cos(m \pi \xi) \sin(n \pi \eta) \\ H \bar{u}_y(\zeta) \sin(m \pi \xi) \cos(n \pi \eta) \\ c_{44}^0 \bar{\sigma}_{zz}(\zeta) \sin(m \pi \xi) \sin(n \pi \eta) \\ \sqrt{c_{44}^0 \varepsilon_{33}} \bar{D}_z(\zeta) \sin(m \pi \xi) \sin(n \pi \eta) \\ c_{44}^0 \bar{\sigma}_{zx}(\zeta) \cos(m \pi \xi) \sin(n \pi \eta) \\ c_{44}^0 \bar{\sigma}_{yz}(\zeta) \sin(m \pi \xi) \cos(n \pi \eta) \\ H \bar{u}_z(\zeta) \sin(m \pi \xi) \sin(n \pi \eta) \\ H \sqrt{c_{44}^0 / \varepsilon_{33}} \bar{\phi}(\zeta) \sin(m \pi \xi) \sin(n \pi \eta) \end{Bmatrix} \exp(i \omega t) \tag{6}$$

where the superscript 0 denotes quantities at $\zeta = 0$.

The substitution of Eq. (6) into Eq. (3) yields

$$\frac{d}{d\zeta} \mathbf{V}_p(\zeta) = \mathbf{M}_p \mathbf{V}_p(\zeta) \tag{7}$$

where $\mathbf{V}_p = [\bar{u}_x \; \bar{u}_y \; \bar{\sigma}_{zz} \; \bar{D}_z \; \bar{\sigma}_{zx} \; \bar{\sigma}_{yz} \; \bar{u}_z \; \bar{\phi}]^T$ denotes the nondimensional state vector for piezoelectric layers, and the coefficient matrix $\mathbf{M}_p$ is expressed in Appendix A.

The solution to Eq. (7) can be obtained as

$$\mathbf{V}_p(\zeta) = \exp[(\zeta - \zeta_1)\mathbf{M}_p] \cdot \mathbf{V}_p(\zeta_1), \quad (\zeta_1 \le \zeta \le \zeta_2) \tag{8}$$

where $\zeta_1 = h_1/H$ and $\zeta_2 = (h_1 + h_2)/H$. Hence, we can establish the following relation

$$\mathbf{V}_p(\zeta_2) = \mathbf{S}_p\mathbf{V}_p(\zeta_1) \tag{9}$$

where $\mathbf{S}_p = \exp[(\zeta_2 - \zeta_1)\mathbf{M}_p]$ is the transfer matrix of the sensor or actuator piezoelectric layers, which can be calculated by the built-in exponential matrix functions of some commercial algebraic manipulation codes such as Mathematica and Matlab.

2.2 Formulations for FGM layers

In a similar way, the state equation for the FGM layers can be derived as:

$$\frac{d}{d\zeta}\mathbf{V}_f(\zeta) = \mathbf{M}_f\mathbf{V}_f(\zeta) \tag{10}$$

where $\mathbf{V}_f = [\bar{u}_x \ \bar{u}_y \ \bar{\sigma}_{zz} \ \bar{\sigma}_{zx} \ \bar{\sigma}_{yz} \ \bar{u}_z]^T$ is the corresponding nondimensional state vector. Deleting the fourth and eighth rows and columns of the forenamed coefficient matrix $\mathbf{M}_p$, one can obtain the sixth-order square matrix $\mathbf{M}_f$, which can be different for FGM I and FGM II. On the other hand, the $\mathbf{M}_f$ varies with the variable ζ resulted from the inhomogeneity of FGMs, which imposes the mathematical difficulty to obtain solution to Eq. (10) analytically. Hence an approximate laminate model (Lee and Jiang 1996) is employed here. That is to say, the FGM layers are divided into N_i ($i = 1, 2$) equal thin fictitious layers, so that the $\mathbf{M}_f$ can be assumed constant within each layer and its value is taken at each mid-plane, i.e.,

$$\mathbf{M}_f(\zeta) = \mathbf{M}_f(\zeta)\Big|_{\zeta = (\zeta_j^0 + \zeta_j^1)/2} \equiv \mathbf{M}_f^{(j)}, \quad (\zeta_j^0 \le \zeta \le \zeta_j^1) \tag{11}$$

where

$$\zeta_j^0 = (j-1)h_1/(N_1H), \ \zeta_j^1 = jh_1/(N_1H) \quad \text{and} \quad j = 1, 2, \ldots, N_1 \quad \text{for FGM I layer,}$$

$$\zeta_j^0 = 1 - (N_2 + 1 - j)h_3/(N_2H), \ \zeta_j^1 = 1 - (N_2 - j)h_3/(N_2H) \ \text{and} \ j = 1, 2, \ldots, N_2 \tag{12}$$
$$\text{for FGM II layer}$$

Obviously, the solution based on the asymptotic laminate model will gradually approach the exact solution of the original FGM layers when the number of layers increases (Bahar 1975, Lee and Jiang 1996, Chen *et al.* 2003b, Liu *et al.* 2003).

By virtue of the laminate model, the solution of Eq. (10) can be obtained within each fictitious homogeneous layer as

$$\mathbf{V}_f(\zeta) = \exp[(\zeta - \zeta_j^0)\mathbf{M}_f^{(j)}] \cdot \mathbf{V}_f(\zeta_j^0), \quad (\zeta_j^0 \le \zeta \le \zeta_j^1) \tag{13}$$

Setting $\zeta = \zeta_j^1$ in Eq. (13) as well as employing the continuity conditions of the state vectors at each fictitious interface yields the following transfer relation between state vectors at the top and bottom surfaces of the FGM layers

$$\mathbf{V}_f(\zeta_1) = \mathbf{S}_{\mathrm{I}}\mathbf{V}_f(0), \quad \mathbf{V}_f(1) = \mathbf{S}_{\mathrm{II}}\mathbf{V}_f(\zeta_2) \tag{14}$$

where $\mathbf{S}_{\mathrm{I}} = \displaystyle\prod_{j=N_1}^{1} \exp[h_1/(H \cdot N_1) \cdot \mathbf{M}_f^{(j)}]$ and $\mathbf{S}_{\mathrm{II}} = \displaystyle\prod_{j=N_2}^{1} \exp[h_3/(H \cdot N_2) \cdot \mathbf{M}_f^{(j)}]$ are the transfer matrices of FGM I and FGM II, respectively; and both are a sixth-order square matrix.

3. Spring-layer model of weak interfaces

The weekly bonding adhesive between the piezoelectric layer and FGM layers is modeled as a linear spring layer (Chen *et al.* 2003a, Chen and Lee 2004b, Chen *et al.* 2004b,c,d). Hence, the mechanical conditions at the two interfaces between the two FGM layers and the piezoelectric actuator or sensor layer are

at $\zeta = \zeta_1$

$$\sigma_{zz}^{\mathrm{I}}(\zeta_1) = \sigma_{zz}^{p}(\zeta_1) = [u_z^{p}(\zeta_1) - u_z^{\mathrm{I}}(\zeta_1)]/R_z^{\mathrm{I}}$$

$$\sigma_{zx}^{\mathrm{I}}(\zeta_1) = \sigma_{zx}^{p}(\zeta_1) = [u_x^{p}(\zeta_1) - u_x^{\mathrm{I}}(\zeta_1)]/R_x^{\mathrm{I}}$$

$$\sigma_{yz}^{\mathrm{I}}(\zeta_1) = \sigma_{yz}^{p}(\zeta_1) = [u_y^{p}(\zeta_1) - u_y^{\mathrm{I}}(\zeta_1)]/R_y^{\mathrm{I}}$$

at $\zeta = \zeta_2$ $\tag{15}$

$$\sigma_{zz}^{\mathrm{II}}(\zeta_2) = \sigma_{zz}^{p}(\zeta_2) = [u_z^{\mathrm{II}}(\zeta_2) - u_z^{p}(\zeta_2)]/R_z^{\mathrm{II}}$$

$$\sigma_{zx}^{\mathrm{II}}(\zeta_2) = \sigma_{zx}^{p}(\zeta_2) = [u_x^{\mathrm{II}}(\zeta_2) - u_x^{p}(\zeta_2)]/R_x^{\mathrm{II}}$$

$$\sigma_{yz}^{\mathrm{II}}(\zeta_2) = \sigma_{yz}^{p}(\zeta_2) = [u_y^{\mathrm{II}}(\zeta_2) - u_y^{p}(\zeta_2)]/R_y^{\mathrm{II}}$$

where the superscripts 'I' 'II' and 'p' denote the quantities of the FGM I layer, the FGM II layer and the piezoelectric layers, respectively; $R_j(j = x, y, z)$ are the compliance coefficients of adhesives at two interfaces. Note that different cases of bonding imperfections will be included when different values of R_z are assigned. For example, choosing $R_z = 0$ as well as keeping R_x and R_y as finite constants corresponds to the slip-type case. For the completely delaminated and completely perfect cases, then $R_j \to \infty$ and $R_j = 0$ respectively.

Combining Eq. (15) with Eq. (6), one can obtain

$$\mathbf{V}_p^{m}(\zeta_1) = \mathbf{P}_{\mathrm{I}}\mathbf{V}_f(\zeta_1), \quad \mathbf{V}_f(\zeta_2) = \mathbf{P}_{\mathrm{II}}\mathbf{V}_p^{m}(\zeta_2) \tag{16}$$

where $\mathbf{V}_p^{m}$ is the mechanical part of $\mathbf{V}_p$, while $\mathbf{P}_{\mathrm{I}}$ and $\mathbf{P}_{\mathrm{II}}$ are the interfacial transfer matrixes defined by

$$\mathbf{P}_i = \begin{bmatrix} 1 & & & & R_x^i c_{44}^0/H & & \\ & 1 & & & & R_y^i c_{44}^0/H & \\ & & 1 & & & & \\ & & & 1 & & & \\ & & & & 1 & & \\ & R_z^i c_{44}^0/H & & & & & 1 \end{bmatrix}, \quad (i = \text{I}, \text{II}) \tag{17}$$

Obviously, the interfacial transfer matrix will be an identity matrix if the interface is perfect.

4. Boundary conditions of piezoelectric layer and the final governing equation

4.1 Electric boundary conditions

When the piezoelectric layer is used for an actuator, then the electric boundary conditions (Ray *et al.* 1992, 1998) are

$$\phi = \phi_1(x, y)\exp(i\omega t) \quad \text{at} \quad \zeta = \zeta_1; \quad \phi = \phi_2(x, y)\exp(i\omega t) \quad \text{at} \quad \zeta = \zeta_2 \tag{18}$$

where ω is the angular frequency of the imposed electric potential which varies harmonically in time. In terms of the Fourier series, one can expand the amplitudes of the applied electric potentials as

$$\phi_k(x, y) = \sum_{m=1}^{\infty} \sum_{n=1}^{\infty} H\sqrt{c_{44}^0/\varepsilon_{33}} f_{mn}^{(k)} \sin(m\pi\xi)\sin(n\pi\eta), \quad (k = 1, 2) \tag{19}$$

where

$$f_{mn}^{(k)} = \frac{4}{H\sqrt{c_{44}^0/\varepsilon_{33}}} \int_0^1 \int_0^1 \phi_k \sin(m\pi\xi)\sin(n\pi\eta) d\xi d\eta \tag{20}$$

are the Fourier coefficients. Connecting Eq. (18) with Eq. (9) yields

$$\bar{D}_z(\zeta_1) = (f_{mn}^{(2)} - S_{88}^p f_{mn}^{(1)} - \mathbf{R}_8^p \cdot \mathbf{V}_p^m(\zeta_1))/S_{84}^p$$

$$\mathbf{V}_p^m(\zeta_2) = \mathbf{L}_p \mathbf{V}_p^m(\zeta_1) + \mathbf{Q}_p \tag{21}$$

where S_{ij}^p are the elements of matrix $\mathbf{S}_p$, $\mathbf{R}_i^p = [S_{i1}^p \ \ S_{i2}^p \ \ S_{i3}^p \ \ S_{i5}^p \ \ S_{i6}^p \ \ S_{i7}^p]$, and

$$\mathbf{L}_p = [\mathbf{C}_1^p \ \ \mathbf{C}_2^p \ \ \mathbf{C}_3^p \ \ \mathbf{C}_5^p \ \ \mathbf{C}_6^p \ \ \mathbf{C}_7^p] - \mathbf{C}_4^p \mathbf{C}_8^p/S_{84}^p$$

$$\mathbf{Q}_p = (f_{mn}^{(2)} - S_{88}^p f_{mn}^{(1)})/S_{84}^p \cdot \mathbf{C}_4^p + f_{mn}^{(1)} \cdot \mathbf{C}_8^p \tag{22}$$

in which $\mathbf{C}_i^p = [S_{1i}^p \quad S_{2i}^p \quad S_{3i}^p \quad S_{5i}^p \quad S_{6i}^p \quad S_{7i}^p]^T$.

If the piezoelectric layer is used for a sensor, then the electric boundary conditions are Ray *et al.* (1992, 1998),

$$\phi = 0 \quad \text{at} \quad \zeta = \zeta_1; \quad D_z = 0 \quad \text{at} \quad \zeta = \zeta_2 \tag{23}$$

In a similar manner, we can derived the following formulas

$$\overline{D}_z(\zeta_1) = -\mathbf{R}_4^p \cdot \mathbf{V}_p^m(\zeta_1)/S_{44}^p$$

$$\mathbf{V}_p^m(\zeta_2) = \mathbf{L}_p\mathbf{V}_p^m(\zeta_1) \tag{24}$$

Finally, the global elastic transfer relation can be derived from Eqs. (14), (16) (21) or (24)

$$\mathbf{V}_f(1) = \mathbf{T}\mathbf{V}_f(0) + \mathbf{Z} \tag{25}$$

where $\mathbf{T} = \mathbf{S}_{\mathrm{II}}\mathbf{P}_{\mathrm{II}}\mathbf{L}_p\mathbf{P}_{\mathrm{I}}\mathbf{S}_{\mathrm{I}}$ and $\mathbf{Z} = \mathbf{S}_{\mathrm{II}}\mathbf{P}_{\mathrm{II}}\mathbf{Q}_p$ for a piezoelectric actuator or $\mathbf{Z} = \mathbf{0}$ for a piezoelectric sensor.

4.2 Mechanical boundary conditions

Consider a laminated plate with its bottom surface tractions-free and its top surface subjected to a dynamic normal mechanical load, $q(x, y)\exp(i\omega t)$. Expand the amplitude $q(x, y)$ as

$$q(x, y) = c_{44}^0 \sum_{m=1}^{\infty} \sum_{n=1}^{\infty} q_{mn}\sin(m\pi\xi)\sin(n\pi\eta) \tag{26}$$

where

$$q_{mn} = \frac{4}{c_{44}^0}\int_0^1\int_0^1 q\sin(m\pi\xi)\sin(n\pi\eta)d\xi d\eta \tag{27}$$

Then the mechanical boundary conditions can be expressed as

$$\overline{\sigma}_{zz} = -q_{mn}, \quad \overline{\sigma}_{zx} = 0, \quad \overline{\sigma}_{zy} = 0 \quad \text{at} \quad \zeta = 0; \qquad \overline{\sigma}_{zz} = 0, \quad \overline{\sigma}_{zx} = 0, \quad \overline{\sigma}_{zy} = 0 \quad \text{at} \quad \zeta = 1 \tag{28}$$

4.3 Final governing equations

Incorporating Eq. (28) into Eq. (25), we obtain

$$\begin{Bmatrix} \overline{u}_x(0) \\ \overline{u}_y(0) \\ \overline{u}_z(0) \end{Bmatrix} = \begin{bmatrix} T_{31} & T_{32} & T_{36} \\ T_{41} & T_{42} & T_{46} \\ T_{51} & T_{52} & T_{56} \end{bmatrix}^{-1} \begin{Bmatrix} T_{33}q_{mn} - z_3 \\ T_{43}q_{mn} - z_4 \\ T_{53}q_{mn} - z_5 \end{Bmatrix} \tag{29}$$

where T_{ij} and z_i are elements of matrix $\mathbf{T}$ and vector $\mathbf{Z}$, respectively. From Eq. (29), the displacement components and subsequently the top mechanical state vector, $\mathbf{V}_f(0) = [\overline{u}_x(0) \quad \overline{u}_y(0) \quad -q_{mn} \quad 0 \quad 0 \quad \overline{u}_z(0)]^T$, can be determined. Now the other two basic state vectors, $\mathbf{V}_p(\zeta_1)$ and

$\mathbf{V}_f(\zeta_2)$, can be determined by the virtue of Eqs. (9), (14), (16) (21) or (24). Finally, each state vector is solved from Eq. (8) or Eq. (13).

If the free vibration is considered, we have $q_{mn} = 0$ in Eq. (26). If the piezoelectric layer is used for an actuator, then $f_{mn}^{(k)} = 0$ in Eq. (19). The requirement of nontrivial solutions to Eq. (29) yields the following frequency equation

$$\begin{vmatrix} T_{31} & T_{32} & T_{36} \\ T_{41} & T_{42} & T_{46} \\ T_{51} & T_{52} & T_{56} \end{vmatrix} = 0 \qquad (30)$$

5. Numerical examples

For numerical calculating, a hybrid plate consisting of one piezoelectric layer bonded with top and bottom surface FGM laminates is investigated, whose thickness ratio is $h_1{:}h_2{:}h_3 = 4{:}2{:}4$, and total thickness-to-span ratio is $a/H = b/H = 4$. The through-thickness inhomogeneity of FGM layers is expressed as an exponential model (Fuchiyama and Noda 1995), i.e.,

$$P_{\mathrm{I}}(\zeta) = P_0 \exp(\kappa_{\mathrm{I}} \zeta), \quad (0 \le \zeta \le \zeta_1)$$

$$P_{\mathrm{II}}(\zeta) = P_1 \exp[\kappa_{\mathrm{II}}(1 - \zeta)], \quad (\zeta_2 \le \zeta \le 1) \qquad (31)$$

where $P_{\mathrm{I}}(\zeta)$ and $P_{\mathrm{II}}(\zeta)$ represents an arbitrary material constant of FGM I and FGM II, respectively, while P_0 and P_1 refer to two homogeneous materials (P_{I} equals P_0 at $\zeta = 0$, and P_{II} equals P_1 at $\zeta = 1$). In the following numerical examples, they are hypothetical and are listed in Table 1. κ_{I} and κ_{II} are named as gradient indexes of FGM I and FGM II, respectively. For the sake of brief, we choose $\kappa_{\mathrm{I}} = \kappa_{\mathrm{II}} = k$ in the following numerical examples. Table 2 lists the material constants ($Ba_2NaNb_5O_{15}$ (Ding and Chen 2001)) of the piezoelectric actuator or sensor. Within these tables, the units of c_{ij}, ε_{ij}, e_{ij} and ρ are 10^{10} N/m², 10^{-11} F/m, C/m² and 10^3 kg/m³, respectively.

In the following numerical examples, the compliance coefficients R_z^{I} and R_z^{II} are assumed both to be zeros to avoid the phenomenon of material penetration at two interfaces (Cheng *et al.* 1996).

Table 1 Material constants of FGM plate

Property	c_{11}	c_{12}	c_{13}	c_{22}	c_{23}	c_{33}	c_{44}	c_{55}	c_{66}	ρ
P_0	65.53	41.74	2.13	36.66	2.05	7.39	2.24	2.59	42.88	2.3
P_1	7.39	2.32	1.87	173.66	2.32	7.39	3.45	1.38	3.45	1.6

Table 2 Material constants of piezoelectric actuator or sensor

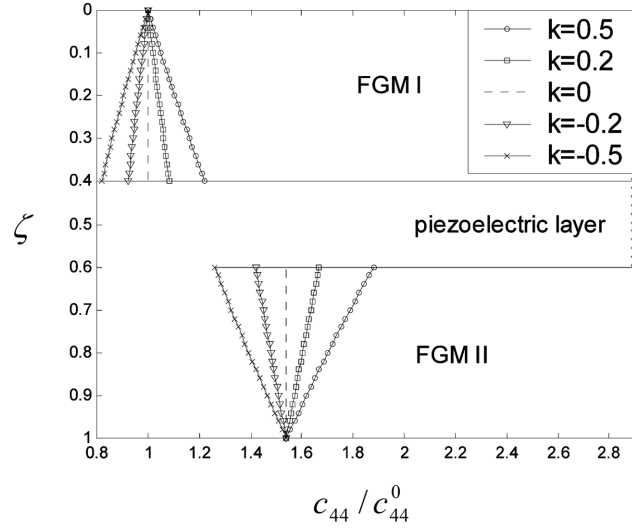| Property	c_{11}	c_{12}	c_{13}	c_{22}	c_{23}	c_{33}	c_{44}	c_{55}	c_{66}
Piezoelectric layer	23.9	10.4	5.0	24.7	5.2	13.5	6.5	6.6	7.6
Property	e_{15}	e_{24}	e_{31}	e_{32}	e_{33}	ε_{11}	ε_{22}	ε_{33}	ρ
Piezoelectric layer	2.8	3.4	−0.4	-0.3	4.3	196	201	28	5.3

Fig. 2 Variation of elastic constant c_{44}/c_{44}^0 through thickness

Besides, we suppose $R_x^I = R_y^{II}$ and $R_x^{II} = R_y^{II}$ for brevity. Two dimensionless parameters are further introduced as $\bar{R}_I = R_x^I c_{44}^0/H$ and $\bar{R}_{II} = R_x^{II} c_{44}^0/H$.

First the variation of material constants in the z direction is investigated. Fig. 2 displays the through-thickness distribution of c_{44}/c_{44}^0 for several values of gradient index k, from which we can see the effect of k on c_{44}/c_{44}^0 is significant.

Next we study the static bending (i.e., $\omega = 0$, time-invariant) of the smart plate. Then a mechanical load, $q(x, y) = c_{44}^0 \sin(\pi\xi)\sin(\pi\eta)$, and electric potentials, $\phi_2 = 0$ and $\phi_1(x, y) = H\sqrt{c_{44}^0/\varepsilon_{33}}\, f_{11}^{(1)}\sin(\pi\xi)\sin(\pi\eta)$, are applied.

Fig. 3 illustrates the effects of compliance coefficients on the through-thickness distribution of some non-dimensional field variables, in which the piezoelectric layer is used for an actuator and $f_{11}^{(1)} = 2$. The gradient index $k = 0.2$ and the data shown in parentheses in these figures correspond to $\bar{R}_I$ and $\bar{R}_{II}$, respectively. Each FGM layer is divided into 20 fictitious layers, and the relative errors are less than 0.4% as compared with the results of 18 fictitious layers. As we can find from these figures that the lateral displacement $\bar{u}_x$ (and also $\bar{u}_y$) is discontinuous across the two bonding interfaces when interfacial imperfection is present. On the other hand, the discontinuity of $\bar{u}_x$ at the FGM I-actuator interface is more significant than that at the FGM II-actuator interface, which can be explained by the larger shear stress induced at the upper interface, as shown in Fig. 3(c). Fig. 3(b) presents the deflection improves with the compliance coefficients, which indicates the reduction of the global stiffness of the hybrid plate due to interfacial imperfection. Because an electric potential is imposed on the top surface of the piezoelectric actuator layer, the deflection of piezoelectric actuator layer varies significantly in the thickness direction.

Fig. 4 demonstrates the effects of gradient index on the through-thickness distribution of these non-dimensional field variables. Unlike in Fig. 3, the piezoelectric layer is now used for a sensor. The compliance coefficients are supposed to be $\bar{R}_I = \bar{R}_{II} = 0.2$, and each FGM layer is also divided into 20 fictitious layers. From these figures, we find the gradient index k can also affect the distributions of these field variables.
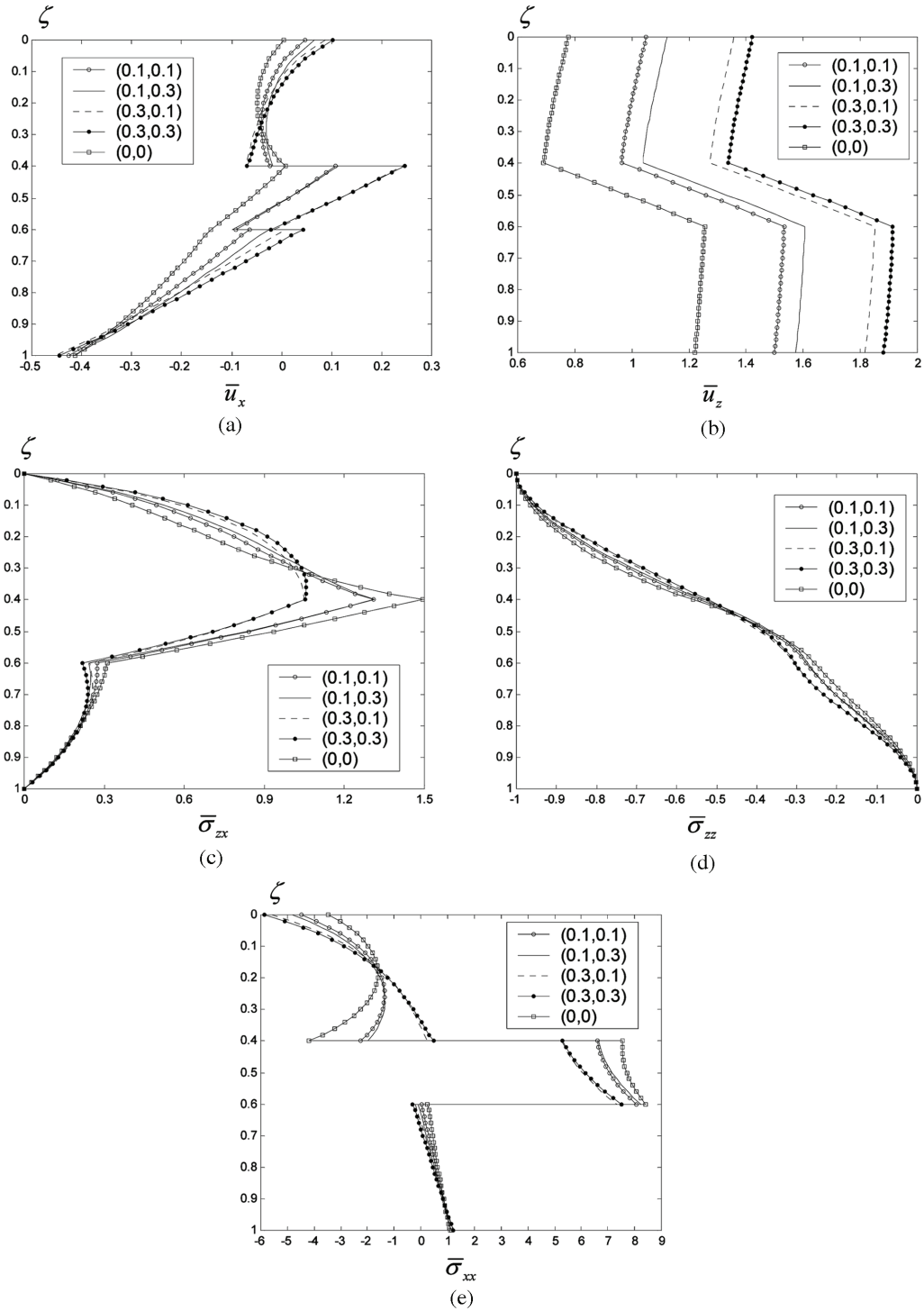
(a)

(b)

(c)

(d)

(e)

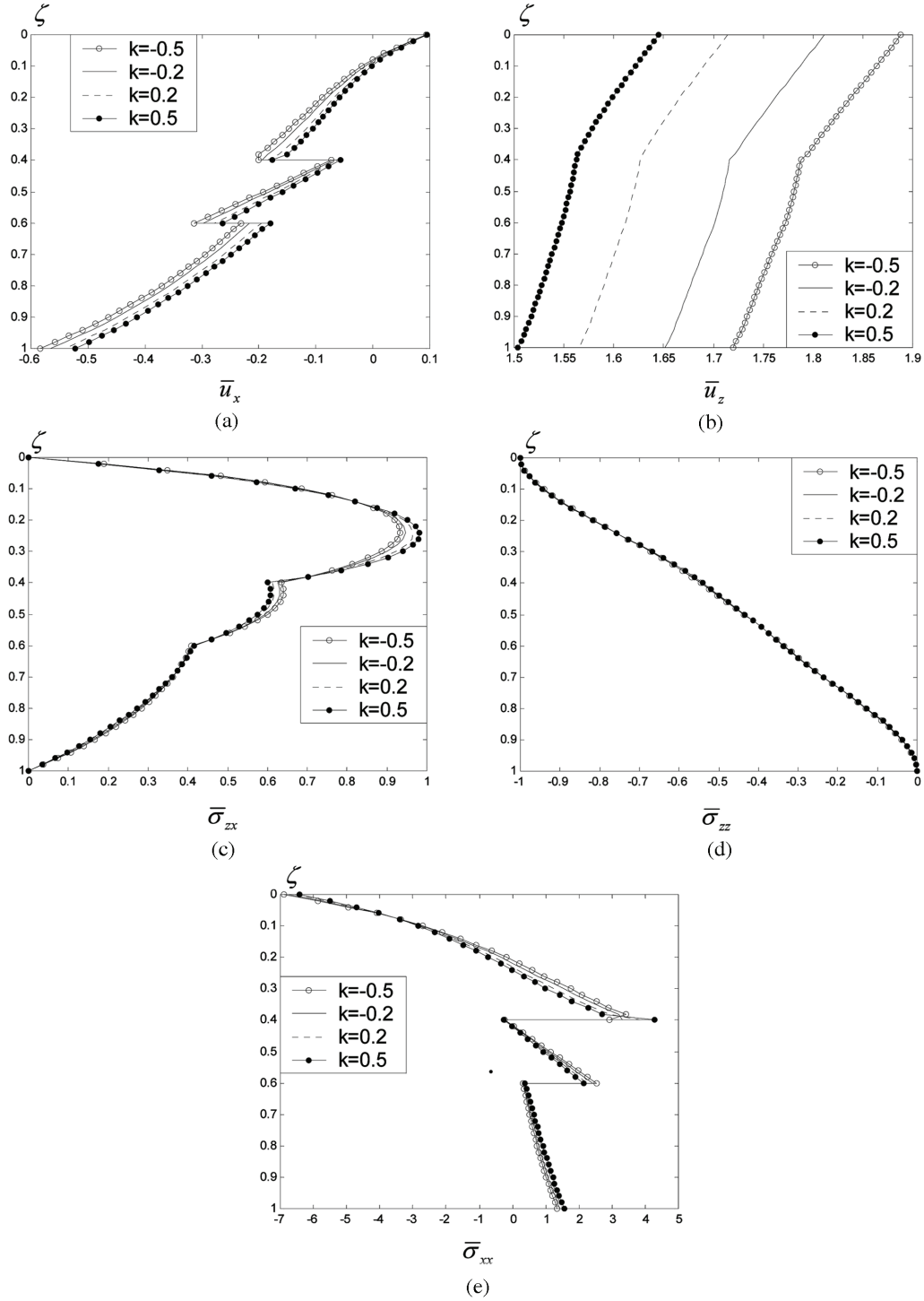Fig. 3 Effect of bonding imperfection on through-thickness distribution

Fig. 4 Effect of gradient index on through-thickness distribution

Table 3 The effects of imperfect interfaces on the dimensionless natural frequency

$\Omega = \omega H \sqrt{\rho^0/c_{44}^0}$		First order	Second order	Third order	Fourth order	Fifth order	Sixth order	Seven order	Eighth order	Ninth order	Tenth order
$R = 0$	actuator	0.8109	2.1784	3.8258	5.2827	5.8405	7.0711	8.2476	10.0457	10.6126	11.2750
	sensor	0.8110	2.1811	3.8317	5.3308	5.8414	7.3426	8.2481	10.0481	10.6204	11.2936
$R = 0.1$	actuator	0.7538	1.9407	3.3023	4.7335	5.0547	7.0124	7.7653	9.2989	9.6415	10.1222
	sensor	0.7539	1.9425	3.3098	4.7716	5.0554	7.2914	7.7688	9.2992	9.6417	10.1231
$R = 0.3$	actuator	0.6898	1.7611	2.8131	3.9034	4.1432	6.9334	7.4193	8.7222	8.8313	9.0092
	sensor	0.6898	1.7622	2.8210	3.9222	4.1579	7.1877	7.4519	8.7263	8.8316	9.0097
$R = 0.5$	actuator	0.6552	1.6830	2.5807	3.4023	3.6871	6.8857	7.3054	8.3755	8.6574	8.7201
	sensor	0.6552	1.6837	2.5878	3.4134	3.7094	7.1063	7.3701	8.3836	8.6575	8.7215

Finally, the free vibration of the present smart plate is investigated. Table 3 lists the first 10 lowest frequencies ($\Omega = \omega H \sqrt{\rho^0/c_{44}^0}$) with different compliance coefficients, where the two compliance coefficients are also supposed to equal, i.e., $\overline{R}_I = \overline{R}_{II} = R$. Besides, the gradient index $k = 0.5$, the wave numbers $m = n = 1$ and each FGM layer is divided into 20 fictitious layers. From these presented data, we can see the natural frequency decreases with the compliance coefficient, which indicates once more the growth of the compliance coefficient will reduce the overall stiffness of the hybrid plate. On the other hand, natural frequencies of actuator and those of sensor are different, the former are little lower than the latter, which should be paid attention in practice.

6. Conclusions

In this paper, the state space method is employed to investigate the static and dynamic problems of a simply supported smart FGM plate. A general linear spring-layer model is introduced to feature the weak interfaces between the piezoelectric laminate and its top and bottom surface FGM layers. With different values of the compliance coefficients in the present model, the interfaces can be from completely perfect to completely debonded. As illustrated in this paper, the treatment of interfacial conditions is very straightforward.

Through the numerical examples, we find the global stiffness of the integrated plate will reduce with the growth of interfacial imperfection, as implied by the increase of deflection and the decrease of natural frequency. On the other hand, there is a little difference of natural frequencies between the cases of piezoelectric sensor and piezoelectric actuator. In a word, the presence of bonding imperfection changes the behavior of the integrated structure, which should be paid much attention to in practice.

Although the SSM is only applicable to plates with some particular configurations and material properties such as those studied in this paper and in Cai *et al.* (2004), Chen *et al.* (2003a), Chen and Lee (2004a,b), Chen *et al.* (2004a,b,c,d), the analytical solutions obtained can be used as benchmarks for clarifying any simplified plate theories and numerical methods for the smart laminates.

Acknowledgments

References

Aboudi, J. (1987), "Damage in composites-modeling of imperfect bonding", *Comp. Sci. Tech.*, **28**, 103-128.

Ali, R., Roy, M.D. and Gopalakrishnan, S. (2004), "An analytical model of constrained piezoelectric thin film sensors", *Sensors and Actuators A: Physical*, **116**, 424-437.

Bahar, L.Y. (1975), "A state space approach to elasticity", *J. Franklin Institute*, **299**, 33-41.

Batra, R.C. and Liang, X.Q. (1997), "The vibration of a rectangular laminated elastic plate with embedded piezoelectric sensors and actuators", *Comput. Struct.*, **63**, 203-216.

Cai, J.B., Chen, W.Q. and Ye, G.R. (2004), "Effect of interlaminar bonding imperfections on the behavior of angle-ply laminated cylindrical panels", *Comp. Sci. Tech.*, **64**, 1753-1762.

Chee, C., Tong, L. and Steven, G.P. (2001), "Static shape control of composite plates using a curvature-displacement based algorithm", *Int. J. Solids Struct.*, **38**, 6381-6403.

Chee, C., Tong, L. and Steven, G.P. (2002), "Piezoelectric actuator orientation optimization for static shape control of composite plates", *Comp. Struct.*, **55**, 169-184.

Chen, W.Q., Cai, J.B. and Ye, G.R. (2003a), "Exact solutions of cross-ply laminates with bonding imperfections", *AIAA J.*, **41**, 2244-2250.

Chen, W.Q., Bian, Z.G. and Ding, H.J. (2003b), "Three-dimensional analysis of a thick FGM rectangular plate in thermal environment", *J. Zhejiang University (Science)*, **4**, 1-7.

Chen, W.Q. and Lee, K.Y. (2004a), "Exact solution of angle-ply piezoelectric laminates in cylindrical bending with interfacial imperfections", *Comp. Struct.*, **65**, 329-337.

Chen, W.Q. and Lee, K.Y. (2004b), "Three-dimensional exact analysis of angle-ply laminates in cylindrical bending with interfacial damage via state-space method", *Comp. Struct.*, **64**, 275-283.

Chen, W.Q., Ying, J., Cai, J.B. and Ye, G.R. (2004a), "Benchmark solution of imperfect angle-ply laminated rectangular plates in cylindrical bending with surface piezoelectric layers as actuator and sensor", *Comput. Struct.*, **82**, 1773-1784.

Chen, W.Q., Ying, J., Cai, J.B. and Ye, G.R. (2004b), "Benchmark solution of laminated beams with bonding imperfections", *AIAA J.*, **42**, 426-429.

Chen, W.Q., Wang, Y.F., Cai, J.B. and Ye, G.R. (2004c), "Three-dimensional analysis of cross-ply laminated cylindrical panels with weak interfaces", *Int. J. Solids Struct.*, **41**, 2429-2446.

Chen, W.Q., Cai, J.B., Ye, G.R. and Wang, Y.F. (2004d), "Exact three-dimensional solutions of laminated orthotropic piezoelectric rectangular plates featuring interlaminar bonding imperfections modeled by a general spring layer", *Int. J. Solids Struct.*, **41**, 5247-5263.

Chen, W.Q., Bian, Z.G., Lv, C.F. and Ding, H.J. (2004e), "3D free vibration analysis of a functionally graded piezoelectric hollow cylinder filled with compressible fluid", *Int. J. Solids Struct.*, **41**, 947-964.

Cheng, Z.Q. and Batra, R.C. (2001), "Thermal effects on laminated composite shells containing interfacial imperfections", *Comp. Struct.*, **52**, 3-11.

Cheng, Z.Q. and Kitipornchai, S. (2000), "Prestressed composite laminates featuring interlaminar imperfection", *Int. J. Mech. Sci.*, **42**, 425-443.

Cheng, Z.Q., Jemah, A.K. and Williams, F.W. (1996), "Theory for multilayered anisotropic plates with weakened interfaces", *J. Appl. Mech.*, **63**, 1019-1026.

Deu, J.F. and Benjeddou, A. (2005), "Free-vibration analysis of laminated plates with embedded shear-mode piezoceramic layers", *Int. J. Solids Struct.*, **42**, 2059-2088.

Ding, H.J. and Chen, W.Q. (2001), *Three Dimensional Problems of Piezoelasticity*, New York, Nova Science Publishers.

Fuchiyama, T. and Noda, N. (1995), "Analysis of thermal stress in a plate of functionally gradient material",

JSAE Rev., **16**, 263-268.

He, X.Q., Ng, T.Y., Sivashanker, S. and Liew, K.M. (2001), "Active control of FGM plates with integrated piezoelectric sensors and actuators", *Int. J. Solids Struct.*, **38**, 1641-1655.

Icardi, U., Di Sciuva, M. and Librescu, L. (2000), "Dynamic response of adaptive cross-ply cantilevers featuring interlaminar bonding imperfections", *AIAA J.*, **38**, 499-506.

Koizumi, M. (1997), "FGM activities in Japan", *Composites B*, **28**, 1-4.

Lee, J.S. and Jiang, L.Z. (1996), "Exact electroelastic analysis of piezoelectric laminate via state space approach", *Int. J. Solids Struct.*, **33**, 977-990.

Li, C.Y. and Weng, G.J. (2002), "Antiplane crack problem in functionally graded piezoelectric materials", *J. Appl. Mech.*, **69**, 481-488.

Liew, K.M., He, X.Q., Ng, T.Y. and Sivashanker, S. (2001), "Active control of FGM plates subjected to a temperature gradient: Modelling via finite element method based on FSDT", *Int. J. Numer. Meth. Eng.*, **52**, 1253-1271.

Liew, K.M., He, X.Q., Ng, T.Y. and Kitipornchai, S. (2003), "Finite element piezothermoelasticity analysis and the active control of FGM plates with integrated piezoelectric sensors and actuators", *Comput. Mech.*, **31**, 350-358.

Liu, G.R., Dai, K.Y., Han, X. and Ohyoshi, T. (2003), "Dispersion of waves and characteristic wave surfaces in functionally graded piezoelectric plates", *J. Sound Vib.*, **268**, 131-147.

Meguid, S.A. and Wang, X.D. (1999), "Wave scattering from cracks and imperfectly bonded inhomogeneities in advanced materials", *Mech. Mater.*, **31**, 187-195.

Noor, A.K. and Burton, W.S. (1990), "Assessment of computational models for multilayered composite shells", *Appl. Mech. Rev.*, **43**, 67-97.

Ootao, Y. and Tanigawa, Y. (2000), "Three-dimensional transient piezothermoelasticity in functionally graded rectangular plate bonded to a piezoelectric plate", *Int. J. Solids Struct.*, **37**, 4377-4401.

Pagano, N.J. (1969), "Exact solutions for composite laminates in cylindrical bending", *J. Comp. Mater.*, **3**, 398-411.

Ray, M.C., Rao, K.M. and Samanta, B. (1992), "Exact analysis of coupled electroelastic behaviour of a piezoelectric plate under cylindrical bending", *Comput. Struct.*, **45**, 667-677.

Ray, M.C., Bhattacharya, R. and Samanta, B. (1998), "Exact solutions for dynamic analysis of composite plates with distributed piezoelectric layers", *Comput. Struct.*, **66**, 737-743.

Roh, J.H. and Kim, J.H. (2003), "Adaptability of hybrid smart composite plate under low velocity impact", *Composites Part B: Engineering*, **34**, 117-125.

Rokhlin, S.I., Wang, L., Xie, B., Yakovlev, V.A. and Adler, L. (2004), "Modulated angle beam ultrasonic spectroscopy for evaluation of imperfect interfaces and adhesive bonds", *Ultrasonics*, **42**, 1037-1047.

Saravanos, D.A. and Heyliger, P.R. (1995), "Coupled layerwise analysis of composite beams with embedded piezoelectric sensors and actuators", *J. Intelligent Mater. Systems and Struct.*, **6**, 350-363.

Shen, H.S. and Liew, K.M. (2004), "Postbuckling of axially loaded functionally graded cylindrical panels with piezoelectric actuators in thermal environments", *J. Eng. Mech.*, **130**, 982-995.

Vel, S.S. and Batra, R.C. (2001), "Exact solution for the cylindrical bending of laminated plates with embedded piezoelectric shear actuators", *Smart Mater. Struct.*, **10**, 240-251.

Yang, J., Kitipornchai, S. and Liew, K.M. (2004), "Non-linear analysis of the thermo-electro-mechanical behaviour of shear deformable FGM plates with piezoelectric actuators", *Int. J. Numer. Meth. Eng.*, **59**, 1605-1632.

Notation

σ_{ij}	: stress components
u_i	: displacement components
ϕ	: electric potential
D_i	: electric displacement components
x, y, z	: Cartesian coordinates

h_1, h_2, h_3 : thickness of FGM I, piezoelectric layer and FGM II, respectively
H, a, b : total thickness, length and width of integrated plate
ξ, η, ζ : dimensionless coordinates, $\xi = x/a$, $\eta = y/b$ and $\zeta = z/H$
c_{ij}, e_{ij}, ε_{ij} : elastic, piezoelectric and dielectric constants
ρ : mass density
m, n : half wave numbers
ω : circular frequency
Ω : dimensionless frequency, $\Omega = \omega H \sqrt{\rho^0/c_{44}^0}$
R_j^i : compliance coefficients of bonding adhesive, $j = x, y, z$, $i = \text{I, II}$

Appendix

The operator matrix **M** and **N** are defined by

$$\mathbf{M} = \begin{bmatrix} \mathbf{0}_{4\times4} & \mathbf{M}_{12} \\ \mathbf{M}_{21} & \mathbf{0}_{4\times4} \end{bmatrix}, \quad \mathbf{N} = \begin{bmatrix} \mathbf{N}_{11} & \mathbf{0}_{3\times4} \\ \mathbf{0}_{2\times4} & \mathbf{N}_{22} \end{bmatrix}$$

$$\mathbf{M}_{12} = \begin{bmatrix} \dfrac{1}{c_{55}} & 0 & -\dfrac{\partial}{\partial x} & -\dfrac{e_{15}}{c_{55}}\dfrac{\partial}{\partial x} \\[2ex] 0 & \dfrac{1}{c_{44}} & -\dfrac{\partial}{\partial y} & -\dfrac{e_{24}}{c_{44}}\dfrac{\partial}{\partial y} \\[2ex] -\dfrac{\partial}{\partial x} & -\dfrac{\partial}{\partial y} & \rho\dfrac{\partial^2}{\partial t^2} & 0 \\[2ex] -\dfrac{e_{15}}{c_{55}}\dfrac{\partial}{\partial x} & -\dfrac{e_{24}}{c_{44}}\dfrac{\partial}{\partial y} & 0 & k_3\dfrac{\partial^2}{\partial x^2}+k_4\dfrac{\partial^2}{\partial y^2} \end{bmatrix}$$

$$\mathbf{M}_{21} = \begin{bmatrix} \rho\dfrac{\partial^2}{\partial t^2}-c_{66}\dfrac{\partial^2}{\partial y^2}+k_2\dfrac{\partial^2}{\partial x^2} & (k_1-c_{66})\dfrac{\partial^2}{\partial x\partial y} & -\dfrac{b_1}{J}\dfrac{\partial}{\partial x} & -\dfrac{b_2}{J}\dfrac{\partial}{\partial x} \\[2ex] (k_1-c_{66})\dfrac{\partial^2}{\partial x\partial y} & \rho\dfrac{\partial^2}{\partial t^2}-c_{66}\dfrac{\partial^2}{\partial x^2}+k_5\dfrac{\partial^2}{\partial y^2} & -\dfrac{b_3}{J}\dfrac{\partial}{\partial y} & -\dfrac{b_4}{J}\dfrac{\partial}{\partial y} \\[2ex] -\dfrac{b_1}{J}\dfrac{\partial}{\partial x} & -\dfrac{b_3}{J}\dfrac{\partial}{\partial y} & \dfrac{\varepsilon_{33}}{J} & \dfrac{e_{33}}{J} \\[2ex] -\dfrac{b_2}{J}\dfrac{\partial}{\partial x} & -\dfrac{b_4}{J}\dfrac{\partial}{\partial y} & \dfrac{e_{33}}{J} & -\dfrac{c_{33}}{J} \end{bmatrix}$$

$$\mathbf{N}_{11} = \begin{bmatrix} -k_2\dfrac{\partial}{\partial x} & -k_1\dfrac{\partial}{\partial y} & \dfrac{b_1}{J} & \dfrac{b_2}{J} \\[2ex] -k_1\dfrac{\partial}{\partial x} & -k_5\dfrac{\partial}{\partial y} & \dfrac{b_3}{J} & \dfrac{b_4}{J} \\[2ex] c_{66}\dfrac{\partial}{\partial y} & c_{66}\dfrac{\partial}{\partial x} & 0 & 0 \end{bmatrix}, \quad \mathbf{N}_{22} = \begin{bmatrix} \dfrac{e_{15}}{c_{55}} & 0 & 0 & -k_3\dfrac{\partial}{\partial x} \\[2ex] 0 & \dfrac{e_{24}}{c_{44}} & 0 & -k_4\dfrac{\partial}{\partial y} \end{bmatrix} \qquad\text{(A.1)}$$

where

$$b_1 = c_{13}\varepsilon_{33} + e_{31}e_{33}, \quad b_2 = c_{13}e_{33} - c_{33}e_{31}, \quad b_3 = c_{23}\varepsilon_{33} + e_{32}e_{33}, \quad b_4 = c_{23}e_{33} - c_{33}e_{32}$$

$$J = c_{33}\varepsilon_{33} + e_{33}^2, \quad k_1 = \frac{c_{13}b_3 + e_{31}b_4}{J} - c_{12}, \quad k_2 = \frac{c_{13}b_1 + e_{31}b_2}{J} - c_{11}$$

$$k_3 = \varepsilon_{11} + e_{15}^2/c_{55}, \quad k_4 = \varepsilon_{22} + e_{24}^2/c_{44}, \quad k_5 = \frac{c_{23}b_3 + e_{32}b_4}{J} - c_{22} \tag{A.2}$$

The nondimensional coefficient matrix $\mathbf{M}_p$ is

$$\mathbf{M}_p = \begin{bmatrix} \mathbf{0}_{4\times4} & \mathbf{M}_{12}^p \\ \mathbf{M}_{21}^p & \mathbf{0}_{4\times4} \end{bmatrix}$$

$$\mathbf{M}_{12}^p = \begin{bmatrix} \dfrac{c_{44}^0}{c_{55}} & 0 & -\lambda_1 & -\lambda_1\dfrac{e_{15}}{c_{55}}\sqrt{\dfrac{c_{44}^0}{\varepsilon_{33}}} \\[3mm] 0 & \dfrac{c_{44}^0}{c_{44}} & -\lambda_2 & -\lambda_2\dfrac{e_{24}}{c_{44}}\sqrt{\dfrac{c_{44}^0}{\varepsilon_{33}}} \\[3mm] \lambda_1 & \lambda_2 & -\Omega^2\dfrac{\rho}{\rho^0} & 0 \\[3mm] \lambda_1\dfrac{e_{15}}{c_{55}}\sqrt{\dfrac{c_{44}^0}{\varepsilon_{33}}} & \lambda_2\dfrac{e_{24}}{c_{44}}\sqrt{\dfrac{c_{44}^0}{\varepsilon_{33}}} & 0 & -\dfrac{k_3\lambda_1^2 + k_4\lambda_2^2}{\varepsilon_{33}} \end{bmatrix}$$

$$\mathbf{M}_{21}^p = \begin{bmatrix} \lambda_2^2\dfrac{c_{66}}{c_{44}^0} - \lambda_1^2\dfrac{k_2}{c_{44}^0} - \Omega^2\dfrac{\rho}{\rho^0} & \lambda_1\lambda_2\dfrac{c_{66} - k_1}{c_{44}^0} & -\lambda_1\dfrac{b_1}{J} & -\lambda_2\dfrac{b_2}{J}\sqrt{\dfrac{\varepsilon_{33}}{c_{44}^0}} \\[3mm] \lambda_1\lambda_2\dfrac{c_{66} - k_1}{c_{44}^0} & \lambda_1^2\dfrac{c_{66}}{c_{44}^0} - \lambda_2^2\dfrac{k_2}{c_{44}^0} - \Omega^2\dfrac{\rho}{\rho^0} & -\lambda_2\dfrac{b_3}{J} & -\lambda_2\dfrac{b_4}{J}\sqrt{\dfrac{\varepsilon_{33}}{c_{44}^0}} \\[3mm] \lambda_1\dfrac{b_1}{J} & \lambda_2\dfrac{b_3}{J} & \dfrac{\varepsilon_{33}c_{44}^0}{J} & \dfrac{e_{33}}{J}\sqrt{c_{44}^0\varepsilon_{33}} \\[3mm] \lambda_1\dfrac{b_2}{J}\sqrt{\dfrac{\varepsilon_{33}}{c_{44}^0}} & \lambda_2\dfrac{b_4}{J}\sqrt{\dfrac{\varepsilon_{33}}{c_{44}^0}} & \dfrac{e_{33}}{J}\sqrt{c_{44}^0\varepsilon_{33}} & -\dfrac{c_{33}\varepsilon_{33}}{J} \end{bmatrix} \tag{A.3}$$

where $\lambda_1 = m\pi H/a$ and $\lambda_2 = n\pi H/b$.